Universiteit
Antwerpen

This item is the archived peer-reviewed author-version of:

Exploring the effects of graphene and temperature in reducing electron beam damage : a TEM and electron diffraction-based quantitative study on Lead Phthalocyanine (PbPc) crystals

Reference:
Jain Noopur, Hao Yansong, Parekh Urvi, Kaltenegger Martin, Pedrazo-Tardajos Adrian, Lazzaroni Roberto, Resel Roland, Geerts Yves Henri, Bals Sara, Van Aert Sandra.- Exploring the effects of graphene and temperature in reducing electron beam damage : a TEM and electron diffraction-based quantitative study on Lead Phthalocyanine (PbPc) crystals
Micron - ISSN 1878-4291 - 169(2023), 103444
Full text (Publisher's DOI): https://doi.org/10.1016/J.MICRON.2023.103444
To cite this reference: https://hdl.handle.net/10067/1960690151162165141

uantwerpen.be
Institutional repository IRUA

Exploring the effects of graphene and temperature in reducing electron beam damage: A TEM and electron diffraction-based quantitative study on Lead Phthalocyanine (PbPc) crystals

Noopur Jain[1,#], Yansong Hao[1,2,#], Urvi Parekh[1], Martin Kaltenegger[3,4], Adrián Pedrazo-Tardajos [1], Roberto Lazzaroni[2], Roland Resel[3], Yves Henri Geerts[4,5], Sara Bals[1,*] and Sandra Van Aert[1,*]

1 Electron Microscopy for Materials Science (EMAT) and NANOlab Center of Excellence, University of Antwerp, 2020 Antwerp, Belgium

2 Laboratory for Chemistry of Novel Materials, Materials Research Institute, University of Mons, 7000 Mons, Belgium

3 Institute of Solid State Physics, Graz University of Technology, 8010 Graz, Austria

4 Laboratory of Polymer Chemistry, Faculty of Science, Université Libre de Bruxelles (ULB), 1050 Brussels, Belgium

5 International Solvay Institutes of Physics and Chemistry, 1050 Brussels, Belgium

# These authors have contributed equally to this work.

*Corresponding authors. Email: Sara.Bals@uantwerpen.be, Sandra.vanaert@uantwerpen.be

Keywords: Electron diffraction, graphene, electron beam damage, Lead Phthalocyanine, cryogenic temperature, organic crystals

Abstract: High-resolution transmission electron microscopy (TEM) of organic crystals, such as Lead Phthalocyanine (PbPc), is very challenging since these materials are prone to electron beam damage leading to the breakdown of the crystal structure during investigation. Quantification of the damage is imperative to enable high-resolution imaging of PbPc crystals with minimum structural changes. In this work, we performed a detailed electron diffraction study to quantitatively measure degradation of PbPc crystals upon electron beam irradiation. Our study is based on the quantification of the fading intensity of the spots in the electron diffraction patterns. At various incident dose rates (e/Å^2/s) and acceleration voltages, we experimentally extracted the decay rate (1/s), which directly correlates with the rate of beam damage. In this manner, a value for the critical dose (e/Å^2) could be determined, which can be used as a measure to quantify beam damage. Using the same methodology, we explored the influence of cryogenic temperatures, graphene TEM substrates, and graphene encapsulation in prolonging the lifetime of the PbPc crystal structure during TEM investigation. The knowledge obtained by diffraction experiments is then translated to real space high-resolution TEM imaging of PbPc.

1 Introduction

Metal phthalocyanines are an important class of organic materials, which have attracted wide interest due to their thermal and chemical stability, semiconductor properties, catalytic activity, etc.[1] Lead phthalocyanine (PbPc) (Figure 1a)[2] is of special interest because of its excellent properties such as thermal and chemical stability,[3] photoconductivity,[4] electrical conductivity,[5] and sensing abilities for various toxic gases.[6] Although most structural investigations on PbPc or other phthalocyanines are done using X-ray diffraction (XRD), the information obtained is usually from a large area and not locally from a single nanometer-sized crystal. On the contrary, transmission electron microscopy (TEM) has the capability to explore the atomic-scale structural information and hence it would, in principle, be an ideal technique to study the atomic structure of PbPc. Unfortunately, the sensitivity of organic materials to degradation under the electron beam is a fundamental limitation of electron microscopy.[7]

Electron beam damage corresponds to the gradual disintegration of the crystal structure during the interaction with the incident electrons. Depending on the material under investigation, electron beam damage can be associated to either elastic or inelastic scattering of electrons during interaction with the material, leading to either knock-on or radiolytic processes, respectively.[7] Knock-on damage corresponds to the displacement of a particular atom depending on the energy of the incident electron and it can be quite substantial for inorganic materials.[8] In contrast, for organic materials, inelastic scattering leads to ionization-based damage in the structure, also called radiolysis.[7] In this paper, we focus on organic PbPc crystals and therefore, our aim is to understand how electron beam damage related to radiolysis can be reduced for these materials.[7,9]

Radiolysis occurs by secondary free radicals that are generated due to inelastic collision of electrons with the material.[7,9] The thermal vibration of atoms and their consequent displacements due to bond breaking leads to a gradual loss of crystallinity in the presence of the electron beam. Studying this loss of crystallinity by high-resolution TEM imaging in a quantitative manner is challenging because of the high electron dose required to obtain an image of the specimen with good signal-to-noise ratio (SNR) and the necessity to finetune the defocus and tilting prior to acquisition. These steps require a substantial electron dose and cause considerable amount of damage in the structure, before even starting to collect

images for further analysis. To overcome these challenges, a quantitative measure of the beam damage that can be used as prior knowledge for imaging experiments is desirable. Electron diffraction has become a popular technique to measure the extent of the beam damage in proteins,[10] organic thin films,[11] and other beam-sensitive materials.[12] Such experiments can be performed for a wide range of electron dose rates with the possibility of using extremely low values i.e., ~10^{-3} e/Å^2/s but still enabling high-quality diffraction patterns at relatively short exposures (order of ms).[13,14] Moreover, unlike imaging in TEM/scanning TEM (STEM) mode, the spot intensities are not affected by sample drift or motion[15] and the effect of the electron beam can be quantified by following the fading intensities of diffraction rings or spots with respect to time or accumulated dose.[11,16–18]

To quantitatively obtain relevant information, it is important to develop a methodology to accurately measure electron beam damage from diffraction experiments. Once the methodology is defined, the quantitative study can be taken forward to investigate various approaches to reduce electron beam damage for beam-sensitive crystals. One of the known protective factors is the use of cryogenic temperature to reduce the secondary processes contributing to radiolysis that depend on thermal vibrations of the atoms.[7,9] It has been established that cryogenic temperatures induce a caging effect where the free radicals generated by inelastic scattering are less mobile and hence cause less damage.[19] In addition, cryogenic temperatures also help in suppressing the secondary reactions that are responsible for further damage. Although improvements in the quality of the images have been shown for biological samples,[7] quantitative evaluation of electron beam damage at cryogenic temperature is still missing for organic crystals such as PbPc.

Another promising approach to reduce beam damage is by depositing the material to be investigated on a graphene grid rather than on a more conventional amorphous carbon grid. It has been found that a graphene substrate improves the dose tolerance of certain materials such as MoS_2.[20,21] A single graphene layer, which is used as a substrate to support the sample, can quench the electronic excitations that are generated by excitations due to the electron beam interaction with the material and can bring the system to ground state.[22] By quenching the mobility of these excited radicals, a graphene layer helps in reducing the extent of electron beam damage. To further reduce beam damage in materials such as MoS_2, two

single-layers of graphene have been used to sandwich the MoS_2.[21] The encapsulation of MoS_2 from both surfaces resulted in a higher degree of protection from the electron beam damage compared to a single-layer of graphene on the exit surface.[21] Here, the exit surface refers to the surface where the electron beam exits the specimen. On the other hand, graphene itself suffers from electron beam damage due to ionization, heating, chemical etching and/or knock-on displacement.[23] Therefore, to use graphene as a protective factor, substantial control over the beam current applied to the sample and the energy of the electrons is required. Beam damage in pristine graphene has been reported to be significantly lower at electron acceleration voltages below 80 kV.[23] Interestingly, for organic crystals, it is known that lowering the acceleration voltage leads to an increase in electron beam damage.[24,25] Due to this trade-off between optimum voltage for the protection of graphene on the one hand and the protection of the organic crystal on the other hand, it is far from straightforward to employ graphene as a protecting layer for organic crystals and the potential for its use needs to be better understood.

In this work, we perform diffraction measurements to quantify the radiation damage of PbPc crystals. Various protection strategies such as the use of a graphene support, graphene encapsulation and cryogenic temperature are used to minimize radiation damage. The effect of dose rate, cumulative dose and acceleration voltage is explored in detail. This study provides a detailed framework to quantify and reduce electron beam damage for PbPc and related organic crystals for future electron microscopy-based studies.

2 Methods

2.1 Sample preparation methods

Lead phthalocyanine (PbPc) was obtained in a powder form after purification by vacuum sublimation. To facilitate the acquisition of reliable electron diffraction patterns and their data processing (explained in Section 3), two different methods were tested to deposit PbPc crystals on the TEM grids. In the first method *i.e.* dropcasting, 1 mg of the PbPc powder was dispersed in 2 mL of solvent (ethanol or chloroform) and sonicated for 10 min. Around 20 µL of the dispersed solution was then dropcast on a

conventional TEM grid and left for overnight drying to remove the excess solvent. The conventional TEM grids are perforated support foils with a pre-defined hole size, shape, and arrangement uniformly spaced holes of 2 µm size on an amorphous carbon mesh. These PbPc crystals lying on the holes are used for the experiments and the conventional grids will be referred to as *C* grids in the remainder of this paper. With this simple and robust method, single crystal diffraction patterns could be observed from individual PbPc crystals (Supplementary Figure S2). Although this preparation method provides the ease of processing diffraction spots from a single crystal of PbPc, we observed that the crystals start rotating under the electron beam, which led to random changes in the intensities of spots (Supplementary Figure S3). This prevented the accurate read-out of the decaying intensities of the diffraction spots. To avoid the random changes in the intensity of diffraction spots while analysing the intensities, we moved on to use PbPc crystals deposited by an alternate method *i.e.* Physical Vapor Deposition (PVD) on the conventional TEM grid. The complete method is described in the Supplementary information (Section S1.1). Two types of PbPc samples were prepared using the PVD setup: one on conventional TEM grids (PbPc/C) and another on graphene-coated TEM grids (PbPc/graphene/C). These in-house prepared graphene TEM grids are conventional grids modified with a single layer of graphene covering the previously empty holes. The graphene grids will be referred to as graphene/C. The PbPc thin film thickness was kept constant at ~20 nm for all experiments to avoid discrepancies in diffraction intensities due to varying thickness of the region under study.[26]

2.2 Graphene coating on TEM grids

Graphene has been used in various configurations (single-layer or multiple layers) to protect materials from electron beam damage. To determine whether the severity of beam damage for PbPc crystals is reduced by using graphene as a support, conventional TEM grids were coated with a single layer of graphene before the deposition of PbPc. The graphene coating can indeed improve the adhesion of the PbPc crystals to the grid, which in turn would help in reducing their rotation under the electron beam.[27,28] Here, a single layer of graphene (Graphenea, Inc, Cambridge, USA) was deposited on the TEM grid using a wet-chemical approach, described in detail in Supplementary Figure S1a (EP4011828A1 patent pending). The intricate process of making graphene coating in-house required the optimization of

etching and cleaning parameters, eventually producing TEM grids covered with a clean single-layer graphene. The successful deposition of graphene was confirmed by observing the hexagonal diffraction spots at a d-spacing of ~2.13 Å. After confirming the presence of graphene on the TEM grid, PbPc is deposited on the graphene/C grids.

2.3 Cryogenic cooling

To assess the effect of cooling on the dose tolerance of PbPc crystals, the TEM grids prepared by PVD were placed in a Fischione cooling holder. The holder is attached to a liquid nitrogen Dewar which was filled during the experiment. The sample was allowed to stabilize for 15 min in the presence of liquid nitrogen before starting the experiment to avoid drift in the sample while acquiring the data.

2.4 Graphene encapsulation of PbPc/graphene/C grids

Here, the PbPc/graphene/C TEM grids were used to deposit another single layer of graphene on top of the PbPc film, resulting in graphene/PbPc/graphene/C TEM grids. Graphene encapsulation is a challenging process that requires a single layer of graphene to float in a solvent before it is deposited on the TEM grid with the sample. This process required various parameters to be optimized in-house before obtaining a clean graphene layer that encapsulates the sample with good coverage. The detailed protocol is described in the Supplementary information (Section S1.2, Figure S1b). The resulting graphene/PbPc/graphene/C grids were confirmed using electron diffraction where two sets of hexagonal spot patterns are observed (one for each graphene layer beneath and above PbPc).

2.5 Diffraction experiments

A Thermo Fischer Scientific Tecnai microscope, operated at 200 kV, was used to acquire videos of fading diffraction patterns from the PbPc sample. Figure 1b shows a TEM image of the thin PVD-grown film with PbPc crystals deposited at a constant thickness. To minimize the electrons interacting with the sample, we used the following procedure: the electron beam was blanked, and the sample was moved randomly. Consequently, the sample was not exposed before recording the first diffraction pattern. Once the recording was started the electron beam was switched on (unblanked). The different dose rates used for this study were obtained by controlling a combination of spot size, condenser

aperture and beam spread in the TEM mode. The various dose rates that were used are: ~11, ~7, ~3 and ~2 e/Å^2/s. The dose rates were determined carefully by measuring the electron counts on the fluorescent screen with uniform illumination. Once the desired dose rate is fixed, the diffraction patterns are collected using a specific camera length of 970 mm and SAED aperture of 10 µm. The beam was spread to expose the selected area uniformly. The integration time for collecting the individual frames was set at 1s. These parameters were kept constant for experiments at a particular dose rate. Multiple videos of

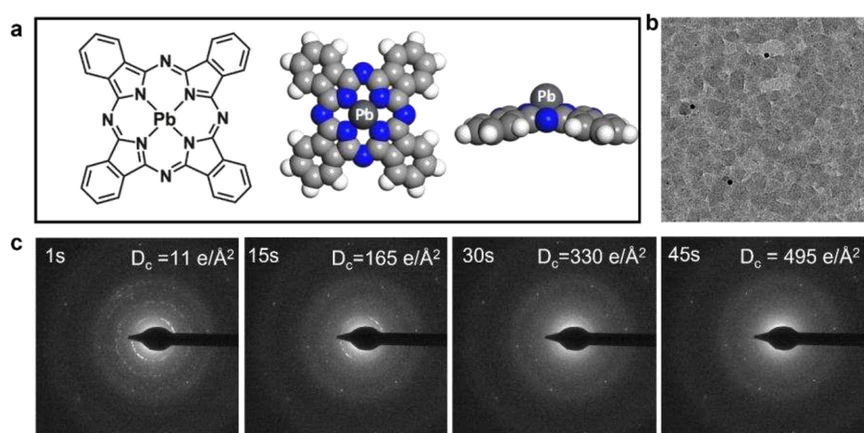

Figure 1. **(a)** Molecular structure of Lead Phthalocyanine (PbPc), **(b)** low magnification bright-field TEM image of PbPc crystals prepared as a film (20 nm thickness) by physical vapor deposition, and **(c)** panel displaying a series of intermediate frames showing disappearing diffraction rings, indicating that the crystals damage from crystalline to amorphous state when exposed to the electron beam for PbPc/graphene/C sample. The experiments were performed at an acceleration voltage of 200 kV and a dose rate of ~11 e/Å^2/s. The time and cumulative dose (D_c) are mentioned for each figure.

disappearing diffraction patterns were collected from different regions. The intensities obtained from different videos at the same dose rate are then averaged to reduce the measurement error. Figure 1c shows snapshots of a time series collected at a dose rate of ~11 e/Å^2/s as an example displaying the fading intensity of the polycrystalline diffraction ring of PbPc. The first diffraction ring for PbPc is used for this study whereas the higher order rings are not analysed because of their high sensitivity to the incoming electrons and the associated fast disappearance at higher dose rates (>2 e/Å^2/s)The procedure was repeated for different dose rates. The acquired diffraction patterns will further be processed to extract and quantitatively analyse how they evolve as a function of dose accumulation.

2.6 Processing of the diffraction data

The intensity of the PbPc diffraction ring is acquired by radially averaging the diffraction pattern.[12] Compared to intensities directly extracted from selected diffraction spots, such a radial averaging

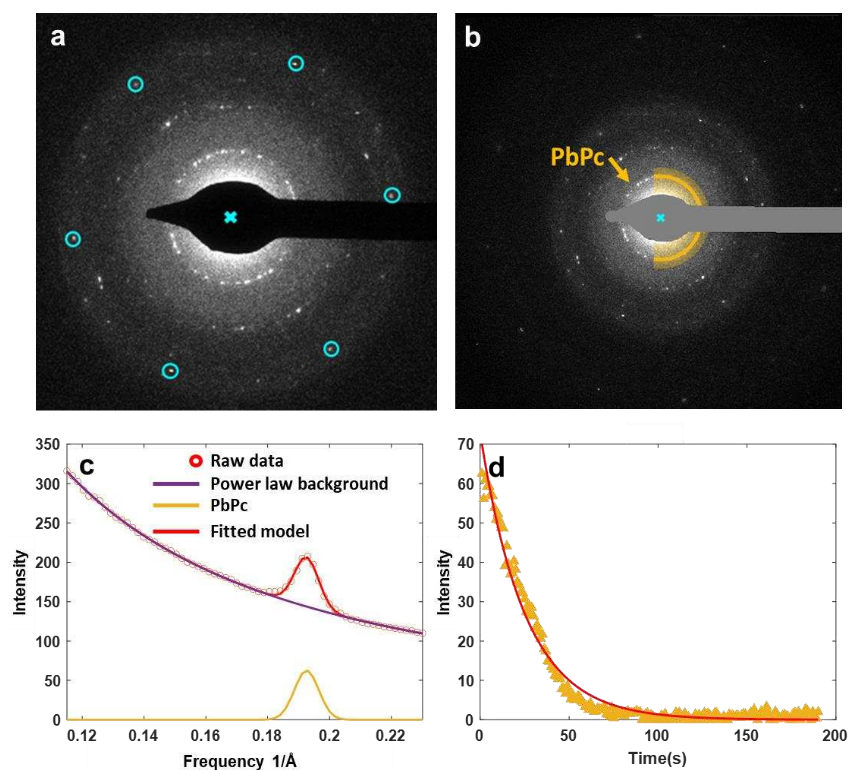

Figure 2. Illustration of the step-by-step processing of the electron diffraction patterns for PbPc/graphene/C samples. **(a)** Determination of the center of the diffraction pattern, **(b)** PbPc diffraction ring to calculate the radial average intensity. The yellow-shaded area shows the range for which the radial average intensity is calculated (from 0.12 Å-1 to 0.23 Å-1) **(c)** Fitting and decomposition of the radial average intensity and **(d)** Plot of the fading intensity of the diffraction ring of PbPc as a function of time. The exponential fitting from Eq.(2) is shown as the red curve.

process provides a more accurate description for the intensity of the diffraction ring. The average intensity is then studied as a function of time, which enables a quantitative evaluation of the electron beam damage of the PbPc crystals. The proposed approach is illustrated in Figure 2.

The first step (Figure 2a) in this procedure is to determine the center of the diffraction pattern and this is accomplished by using the Pets2 software package.[29] Originally, this software was developed for reconstructing the reciprocal lattice of crystals from electron diffraction tomography datasets. In this

study, we use Pets2 to determine the center of diffraction patterns, which is achieved by automatic detection of the Friedel pairs. Such automatic detection is very helpful since the beam position varies between each frame of the diffraction video. Consequently, it is not feasible to manually determine the center of the diffraction pattern frame by frame. An example is illustrated in Figure 2a, where the estimated center is indicated as a cyan-coloured cross. The black arrow in the middle of the figure is the beam stopper, which is used in all experiments to protect the detector from overexposure and saturation. The accuracy of determining the center is demonstrated by the hexagonal diffraction spots of graphene (highlighted by cyan circles), which are distributed symmetrically around the center.

Next, the beam stopper is manually covered with a mask in the diffraction pattern corresponding to the grey region in Figure 2b. The pixel values in this region are not used in the following calculations, whereas the remaining diffraction pattern is radially averaged using an in-house developed Matlab script. This averaging is performed for a range of frequencies around the diffraction ring of PbPc corresponding to the highlighted yellow ring in Figure 2b. Figure 2c shows the calculated radial average intensity where the raw values are represented by the red circles. To quantitatively analyze the degrading intensity of the PbPc diffraction ring, a model is fitted to these raw values using a non-linear least squares method that is implemented in Matlab (*lsqnonlin* command). This model consists of two components, including a Gaussian describing the diffraction intensity from the PbPc crystals and a power law describing the background:

$$I = ae^{\frac{-(x-b)^2}{2c^2}} + Dx^{-\gamma} \qquad \text{(Eq. 1)}$$

Here, x is the distance to the center of the diffraction pattern. The intensity of the PbPc signal is described by the height a of the corresponding Gaussian peak; b and c represent the position and width of the Gaussian peak, respectively. The parameters D and γ describe how the background changes as a function of distance from the center. The fitted model is represented by the red line in Figure 2c, whereas the Gaussian peak for the PbPc crystals and the power law background are shown in yellow and violet, respectively. The excellent quality of the fit confirms the validity of the model to describe the radial average intensity and to extract the contribution from the PbPc crystals.

This radial average intensity profile is calculated for each diffraction pattern of the diffraction video. The intensity contribution from the diffraction of the PbPc crystals, given by the parameter a, is then calculated as a function of time *t* (total recording time of the video, Figure 2d). Next, the extracted intensities are normalized with respect to the initial intensity and then fitted to the following exponential decay function *f_a(t)*:

$$f_a(t) = A \exp(-R_0 t) \qquad \text{(Eq. 2)}$$

where *f_a(t)* is the normalized intensity at time *t, A* is the initial normalized intensity of the PbPc diffraction ring and R_0 is the decay rate (1/s). The explicit determination of the decay rate allows us to

quantitatively compare the beam damage rate of PbPc crystals under different experimental conditions. The cumulative dose (e/Å^2) corresponds to the total dose accumulated on the sample at a particular time during the acquisition and is calculated by multiplying the dose rate by the duration (t) of the diffraction video.

3 Results and Discussion

'Overview dark-field HAADF-STEM images of PbPc crystals grown by PVD are shown in supplementary Figure S4. It is evident that the crystal size (20-50 nm) of PbPc remains in the similar range on C grid, graphene grid and in between two graphene layers. The orientation of the crystals can differ within one specimen as this aspect is not controlled during the deposition. Diffraction time series at different experimental conditions were collected at varying dose rates. Similar to Figure 1c showing snapshots of a diffraction video collected at 11 e/Å^2/s, other diffraction videos (Supplementary Figure S5) were collected for PbPc/graphene/C (at cryogenic temperature), graphene/PbPc/graphene/C and PbPc/C sample at dose rates of ~7, ~3 and ~2 e/Å^2/s at 200 kV. The diffraction videos were processed and analyzed (as explained in *Section 2.6*). The example fitting of raw data for each individual case is shown in Supplementary Figure S7-S10. The results obtained at different dose rates and while applying different protective strategies are explained in the next section.

3.1 Protective factors

3.1.1 Graphene substrate

The diffraction videos were collected for the PbPc/graphene/C samples at fixed dose rates of ~11, ~7, ~3, and ~2 e/Å^2/s and quantitatively analysed. Figure 3(a) shows the trends of the decay rate (1/s) with respect to increasing dose rate (e$^-$/Å^2/s) to compare various protective strategies with the pristine PbPc/C samples (without protection). While the corresponding trend of the critical dose for each applied protective strategies is shown in Figure 3(b). The protective effects from graphene substrate, cryogenic cooling and graphene encapsulation are clearly demonstrated in both cases. For the decay rate, The

black line shows the behaviour of PbPc/C at different dose rates. The effect of the graphene substrate on the electron beam damage of PbPc can be seen by the decay rate trend shown in blue for PbPc/graphene/C. Without the graphene layer on the conventional grid, the PbPc/C samples tend to undergo beam damage significantly faster as compared to PbPc on a graphene/C grid. As an example, at a dose rate of 11 e/Å^2/s, PbPc degrades at a decay rate of 0.092 1/s on a C grid and a rate of 0.079 1/s on graphene/C grids, which shows that PbPc is protected by the graphene support. This already proves

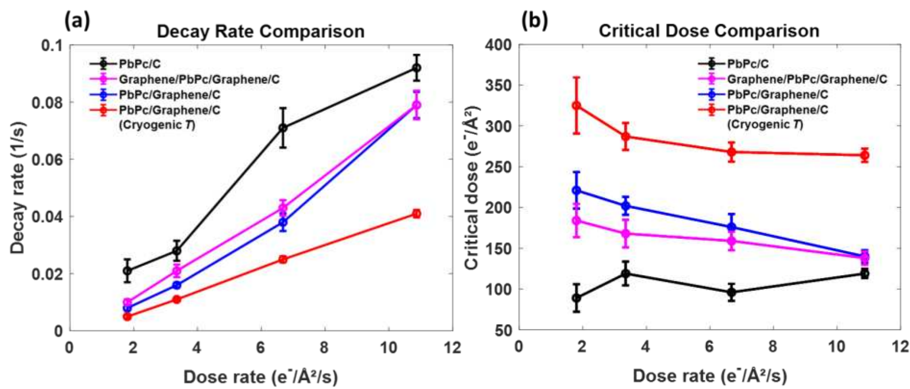

Figure 3. (a) Decay rate (1/s) as a function of the dose rate (e/Å^2/s) at an acceleration voltage of 200 kV. For all dose rates, the diffraction study of PbPc/graphene/C samples at cryogenic temperature (*red line*) shows the slowest decay rates whereas the PbPc/C samples (*black line*) show the fastest decay rate. PbPc/graphene/C at room temperature (*blue line*) shows a reduced decay rate as compared to the PbPc/C (*black line*) but the protection factor is lower than that at cryogenic temperature (*red line*). Graphene/PbPc/graphene/C (*pink line*) shows a decay rate similar to that of PbPc/graphene/C. The respective trend for critical dose vs. dose rate is shown in panel (b).

that covering the exit surface of the PbPc layer with a layer of graphene reduces the damage processes. The exceptional properties of graphene such as thermal and electrical conductivity, are likely responsible for the dissipation of accumulated charge or heat under the beam.[30] Graphene therefore helps in mitigating radiolysis processes that are caused by electronic excitations and charging. Based on these results showing protection with graphene-coated C grids for all dose rates, we will use PbPc/graphene/C grids for all further experiments instead of PbPc/C grids.

3.1.2 Cryogenic temperature

As shown in Figure 3, a graphene substrate already reduces the electron beam sensitivity for PbPc at 200 kV. An additional protective strategy would be to combine the graphene substrate with the use of

cryogenic temperature and will be discussed in this section. To assess the effect of cooling on the dose tolerance of PbPc crystals, the PbPc/graphene/C TEM grids with PbPc deposited by PVD were placed in a cooling holder (Fischione) and liquid nitrogen was filled in the attached dewar. The diffraction patterns were collected at dose rates ~11, ~7, ~3, and ~2 e/Å^2/s. A quantitative evaluation is shown in Figure 3(a) (*red line*) where the calculated decay rate (1/s) is plotted as a function of dose rate (e/Å^2/s). When cooling the sample, the degradation of the PbPc crystals under the electron beam is reduced by a factor of 2.24 in terms of decay rate (decay rate of 0.092 1/s for PbPc/C sample and 0.041 1/s at cryogenic temperature at a dose rate of ~11 e/Å^2/s). Cryogenic cooling thus provides an additional protection factor of about 2 when compared with the graphene/PbPc/C samples at room temperature. This protective factor introduced by cooling the sample is well-known and has been used for multiple specimens.[19,31] For PbPc, cooling certainly increases the dose tolerance since the underlying damage mechanism is radiolysis and a lower temperature reduces the diffusion of the secondary radicals generated during interaction with the electron beam.[32]

Though promising, cryogenic cooling of PbPc samples also has drawbacks such as the formation of ice crystals which can induce drift of the sample while imaging as well as the appearance of extra diffraction spots (Supplementary Figure S11(b-c)).[33] It is therefore crucial to understand and develop other methods to reduce beam damage for PbPc and similar organic crystals without compromising SNR and suffering drift of the sample due to the formation of ice crystals.[22]

3.1.3 Graphene encapsulation

We already observed an enhanced resistance to beam damage by PbPc crystals when they are deposited on a single layer of graphene, compared to the pristine C grids. A full encapsulation of the PbPc crystals between two layers of graphene could further result in additional advantages, as observed successfully with MoS_2 in the literature.[21] The diffraction videos were collected from the graphene encapsulated (GE) samples and were processed in the same way as described above. We dried the TEM grid after graphene encapsulation for 48 hours overnight at 100 ^oC to remove the trapped water/moisture in the graphene pocket, if any, after graphene encapsulation was done. The diffraction experiments were again performed using these GE samples and the decay rates were determined.

From Figure 3, it appears that the protection factor of the graphene/PbPc/graphene/C encapsulated samples (*pink line*) remains very close to the PbPc/graphene/C samples (*blue line*). A possible reason for the lack of further improvement can be that the graphene layer is prone to knock-on damage at 200 kV, at which the above-mentioned diffraction experiments were performed. The knock-on damage of graphene has been studied in the past which provides a quantitative description of its cross-section as a function of acceleration voltage.[34] Following this strategy, we have calculated the knock-on displacement cross section for graphene at 200kV, which is σ_d = 13.3 barn. The corresponding critical electron dose D_c (=e/σ_d) for the knock-on displacement in graphene equals to 1.2×10^4 C/cm^2 (Same value obtained in Egerton, R. F. (2012).[35] For all graphene-encapsulated samples examined at 200kV, the critical dose where PbPc crystals get damaged is below the D_c. Therefore, the encapsulating graphene is not expected to undergo any knock-on damage. In this sense, the lack of protection strongly suggests that the graphene encapsulation should not be used blindly to protect the organic crystals, like PbPc, from beam damage in TEM. To have a better understanding of the beam damage for PbPc with graphene encapsulation, acceleration voltages of 80 kV and 30 kV were also investigated. The example fitting of raw data for 80 kV and 30 kV is shown in Supplementary Figure S12 and S13, respectively.

Commented [YH1]: Add citation

Figure 4a shows the diffraction intensity degradation as a function of time (s) and acceleration voltage for a dose rate of ~11 e/Å^2/s. Similar curves were also obtained at other dose rates (~7, ~3, ~2 e/Å^2/s) and are shown in the Supplementary Figure S14. At each dose rate, a clear trend is followed, with graphene showing a slightly positive protection effect at 30 kV but showing no effect at 80 kV and a negative effect at 200 kV.

These qualitative observations are translated to quantitative information by obtaining the decay rates and critical dose for each condition. Here, the critical dose (e/Å^2) is defined as the cumulative dose at which the intensity of the diffraction ring reduces to 1/e of the initial intensity (in the first frame).[7,18,19] The effect of different acceleration voltages on the decay rate and critical dose of PbPc/graphene/C are shown in Figure 4b and 4c, respectively. At 80 kV, the PbPc/graphene/C samples underwent damage at a higher decay rate as compared to 200 kV for all the dose rates examined. As an example, the PbPc/graphene/C sample at 80 kV decayed with a rate of 0.026 1/s as compared to a decay rate of 0.008

1/s at 200 kV for the same electron dose rate (at ~2 e/Å^2/s). At the same dose rate, the PbPc/graphene/C sample at 30 kV showed even less electron beam tolerance, *i.e.* a decay rate of 0.130 1/s at ~2 e/Å^2/s.

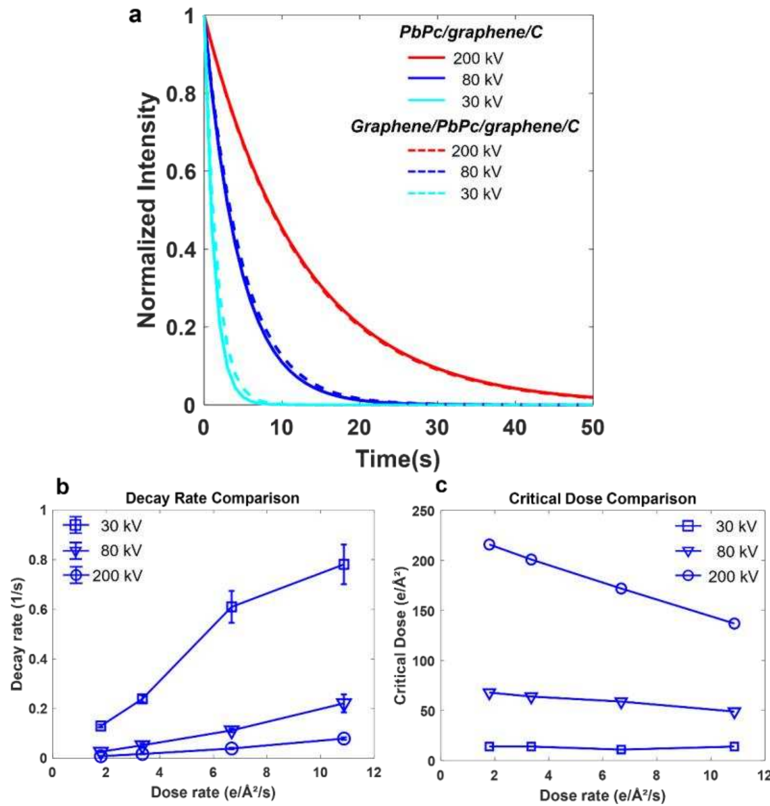

Figure 4. (a) Normalized intensity of the diffraction ring as a function of time showing the effect of graphene encapsulation at different acceleration voltages at a dose rate of 11 e/Å^2/s. **(b)** Decay rate as a function of dose rate for PbPc/graphene/C samples at 30, 80 and 200 kV, and **(c)** critical dose (e/Å^2) as a function of dose rate (e/Å^2/s) at 30, 80 and 200 kV for the PbPc/graphene/C samples.

Although graphene encapsulation protects PbPc at 30 kV, it is not ideal to image PbPc at 30 kV as the crystal itself damages at a much faster rate compared to 200 kV. Therefore, the maximum information during imaging of PbPc could be obtained at 200 kV. Moreover, the difference in the absolute values of intensity of the diffracted beam is not critical for the experiments shown as the normalized intensities (A/A_o) are used to plot the decay curve and calculate the decay rate. Therefore, the recorded changes in the intensity of diffraction spots are always relative to the initial intensity.

3.2 Dose-rate effect

Figure 4c shows the trend of the critical dose (e/Å^2) with respect to the increasing dose rate (e/Å^2/s). An interesting observation that can be derived from Figure 4c is that the electron beam damage not only depends on the cumulative dose (e/Å^2) collected on the sample but also on the dose rate (flux, e/Å^2/s). This effect of dose-rate is more impinging on the sample at 200 kV as compared to 80 kV and almost no effect is seen at 30 kV. We hypothesize that the effect at 200 kV is higher because the interaction of the high-energy electrons with the sample is shorter and an increase in the flux of electrons (dose rate) can still accelerate the decay rate by increasing the formation of secondary radicals that contribute to radiolysis. On the other hand, at 30 kV, the damage with a minimum number of electrons (dose rate: 2 e/Å^2/s) is already so large that increasing the dose rate does not affect the decay rate. Clearly, the dose rate is a critical factor to describe damage, together with the cumulative dose. The probable reasoning proposed is that beam damage occurs as a result of charging and the consequent development of an electric field within the specimen.[36,37] With increasing dose rate, the development of an electric field increases, and damage is enhanced. It is also expected that inelastic processes increase with decreasing beam energy.[7,38]

Our observations at 30 kV and 80 kV suggest that due to such a high degree of damage, the effect of the dose rate is not as clear as in the case of 200 kV. In short, we can identify the response of the system under irradiation, but we do not have a complete understanding of the underlying physical mechanisms responsible for the beam damage. Nevertheless, identifying and understanding the implications of critical dose-rate behaviour on electron beam damage is important for studying organic crystals such as PbPc using TEM.

3.3 High-resolution TEM imaging

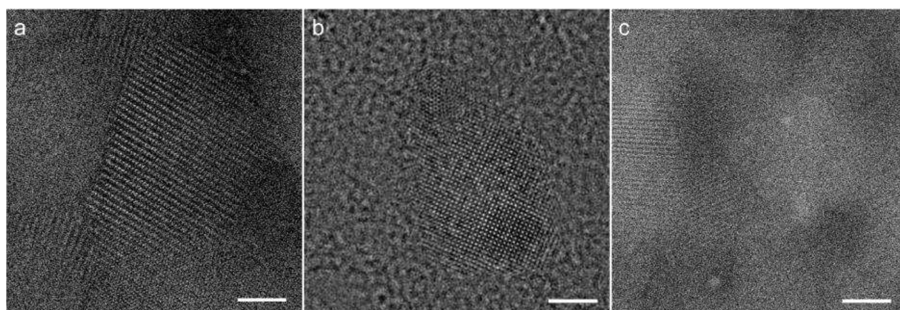

Figure 5: High-resolution TEM images acquired at 300 kV and a cumulative dose of ~50 e/Å^2 for (a) PbPc/C, (b) PbPc/graphene/C and (c) PbPc/graphene/C at cryogenic temperature. Scale bar is 2 nm. The respective FFTs are shown in Supplementary Figure S15.

Once the optimized settings from the diffraction studies resulting in minimum damage were obtained, we performed real-space TEM imaging experiments to directly translate the knowledge from diffraction experiments. To provide the best working conditions for the image-corrector installed in a Thermo Fisher Titan EM, and obtain atomic resolution, we perform the imaging experiments at 300 kV on the PbPc crystals with different protective strategies employed. Since the relative trend for electron beam damage is now understood at different voltages from diffraction, the relative trend can be translated to 300 kV. For bright-field imaging experiments, the dose rate was set at ~12 e/Å^2/s and an exposure time of 4s. add here Figure 5 shows the high-resolution images at a cumulative dose of ~50 e/Å^2 for (a) PbPc/C, (b) PbPc/graphene/C and (c) PbPc/graphene/C at cryogenic temperature. As shown in Figure 5a, for C grids (without graphene), the TEM image provides atomically resolved information, but the beam damage starts building up even during the first frame of acquisition: the atomic columns in one part of the image are resolved with good contrast but other parts show damage to the crystallinity of the PbPc. Next, PbPc/graphene/C samples were imaged at high-resolution. As can be seen in Figure 5b, the structure is imaged with at 300 kV where the Fourier transform indicates the information transfer to 1.2 Å. A comparison between Figure 5a and b clearly shows that the graphene support is providing enhanced protection to the PbPc crystals against beam damage at 300 kV even at half of the critical dose obtained at 200 kV. It is also worth mentioning that though it is unclear if graphene protects the

entire crystal or only the surface, the disappearance of all the spots in the diffraction pattern clearly indicates that all the crystallinity from the selected area of the specimen has disappeared due to damage.

Next, we image the PbPc crystals under the best possible conditions (as observed in diffraction experiments) for reducing beam damage, *i.e.,* at cryogenic temperature. Although the diffraction experiments show that the cryogenic temperature provides the best protection against beam damage, the TEM imaging at high-resolution suggests that the translation from diffraction to real space is not direct. As shown in Figure 5c, the formation of ice crystals during imaging restricts us from obtaining useful data at high-resolution. The presence of ice crystals does not hinder the diffraction measurements because the diffraction spots for ice do not interfere with the diffraction ring of PbPc that is used for the analysis (Supplementary Figure S11). The real space TEM imaging in turn proves that the best resolution and image quality was achieved for the graphene/C grids where the background noise is reduced, since the thin graphene support helps in enhancing the signal-to-noise ratio (Figure 5b). This observation of enhanced image quality of the sample deposition by using graphene is also observed in literature studies done previously.[21,22,39] On the other hand, contrary to the diffraction studies showing promising protection against beam damage at cryogenic temperature, the real space imaging fails due to the ice formation.

4 Conclusions

In this work, we present a detailed quantitative analysis of electron beam damage induced by the electron beam for PbPc crystals. Additionally, we elaborate on the practical aspects such as sample preparation and the substrate used for imaging that make such a study challenging. As seen through diffraction studies, a combination of a graphene substrate and cryogenic cooling was found to be an ideal way to protect PbPc from electron beam damage. Moreover, it was found that the dose rate is a critical factor along with the cumulative dose that influences the electron beam damage. We also provide an in-depth analysis of protection from graphene (substrate and encapsulation). Unlike the diffraction studies, the TEM imaging results in turn show that cryogenic temperature is not ideal for imaging PbPc and instead graphene substrate allows for a more practical and better way of imaging PbPc. Through analysis at different acceleration voltages, we find that graphene encapsulation cannot

be used blindly to protect organic crystals like PbPc from electron beam damage and instead a single layer of graphene at the exit surface provided better protection against electron beam damage. Our approach to analyse the electron beam damage of PbPc crystals under various experimental conditions can provide a framework for future studies to optimize high-resolution imaging conditions for beam-sensitive materials.

Acknowledgements

This work is supported by FWO and FNRS within the 2Dto3D network of the EOS (Excellence of Science) program (grant number 30489208) and ERC-CoGREALNANO-815128 (to Prof. Dr. Sara Bals). N.J. would like to thank Dr. Kunal S. Mali and Dr. Da Wang for useful and interesting discussions on sample preparation procedures.

References

1. McKeown, N. B. *Phthalocyanine materials: synthesis, structure and function*. (Cambridge university press, 1998).

2. Hao, Y. *et al.* From 2D to 3D: Bridging Self-Assembled Monolayers to a Substrate-Induced Polymorph in a Molecular Semiconductor. *Chem. Mater.* **34**, 2238–2248 (2022).

3. Collins, R. A. & Belghachi, A. Structural properties of lead phthalocyanine thin films. *Mater. Lett.* **8**, 349–352 (1989).

4. Mohan Kumar, T. M. & Achar, B. N. Synthesis and characterization of lead phthalocyanine and its derivatives. *J. Organomet. Chem.* **691**, 331–336 (2006).

5. Melville, O. A., Lessard, B. H. & Bender, T. P. Phthalocyanine-Based Organic Thin-Film Transistors: A Review of Recent Advances. *ACS Appl. Mater. Interfaces* **7**, 13105–13118 (2015).

6. Ho, K. C., Chen, C. M. & Liao, J. Y. Enhancing chemiresistor-type NO gas-sensing properties using ethanol-treated lead phthalocyanine thin films. *Sensors Actuators B Chem.* **108**, 418–426 (2005).

7. Egerton, R. F., Li, P. & Malac, M. Radiation damage in the TEM and SEM. *Micron* **35**, 399–409 (2004).

8. Jiang, N. Electron beam damage in oxides: A review. *Reports Prog. Phys.* **79**, (2015).

9. Hobbs, L. W. Transmission Electron Microscopy of Extended Defects in Alkali Halide Crystals. *Surf Defect Prop Solids* **4**, 152–250 (1975).

10. Ophus, C. *et al.* Reducing Electron Beam Damage with Multipass Transmission Electron Microscopy. *Microsc. Microanal.* **23**, 1794–1795 (2017).

11. Guo, C. *et al.* Probing Local Electronic Transitions in Organic Semiconductors through Energy-Loss Spectrum Imaging in the Transmission Electron Microscope. *Advanced Functional Materials* vol. 25 6071–6076 (2015).

12. Leijten, Z. J. W. A., Keizer, A. D. A., De With, G. & Friedrich, H. Quantitative Analysis of Electron Beam Damage in Organic Thin Films. *J. Phys. Chem. C* **121**, 10552–10561 (2017).

13. Henderson, R. & Glaeser, R. M. Quantitative analysis of image contrast in electron micrographs of beam-sensitive crystals. *Ultramicroscopy* **16**, 139–150 (1985).

14. B., D. & E., J. Low-Dose Imaging Techniques for Transmission Electron Microscopy. *Transm. Electron Microsc.* (2012) doi:10.5772/36614.

15. Typke, D., Gilpin, C. J., Downing, K. H. & Glaeser, R. M. Stroboscopic image capture: Reducing the dose per frame by a factor of 30 does not prevent beam-induced specimen movement in paraffin. *Ultramicroscopy* **107**, 106–115 (2007).

16. Glaeser, R. M. Limitations to significant information in biological electron microscopy as a result of radiation damage. *J. Ultrasructure Res.* **36**, 466–482 (1971).

17. Eggeman, A. S., Illig, S., Troisi, A., Sirringhaus, H. & Midgley, P. A. Measurement of molecular motion in organic semiconductors by thermal diffuse electron scattering. *Nat. Mater.* **12**, 1045–1049 (2013).

18. Hayashida, M., Kawasaki, T., Kimura, Y. & Takai, Y. Estimation of suitable condition for observing copper-phthalocyanine crystalline film by transmission electron microscopy. *Nucl. Instruments Methods Phys. Res. Sect. B Beam Interact. with Mater. Atoms* **248**, 273–278 (2006).

19. Hayward, S. B. & Glaeser, R. M. Radiation damage of purple membrane at low temperature. *Ultramicroscopy* **4**, 201–210 (1979).

20. Zan, R. *et al.* Control of Radiation Damage in MoS 2 by Graphene Encapsulation. (1016) doi:10.1021/nn4044035.

21. Algara-Siller, G., Kurasch, S., Sedighi, M., Lehtinen, O. & Kaiser, U. The pristine atomic structure of MoS2 monolayer protected from electron radiation damage by graphene. *Appl. Phys. Lett.* **103**, (2013).

22. Pantelic, R. S., Meyer, J. C., Kaiser, U. & Stahlberg, H. The application of graphene as a sample support in transmission electron microscopy. *Solid State Commun.* **152**, 1375–1382 (2012).

23. Rummeli, M. H. *et al.* New Frontiers in Electron Beam–Driven Chemistry in and around Graphene. *Adv. Mater.* **31**, 1–22 (2019).

24. Stevens, M. R., Chen, Q., Weierstall, U. & Spence, J. C. H. Transmission Electron Diffraction at 200 eV and Damage Thresholds below the Carbon K Edge. *Microsc. Microanal.* **6**, 368–379 (2000).

25. Kobayashi, K. & Sakaoku, K. The Changes of Polymer Crystals due to Irradiation with Electrons Accelerated at Various Voltages (Special Issue on Electron Microscopy). *Bull. Inst. Chem. Res. Kyoto Univ.* **42**, 473–493 (1965).

26. Egerton, R. F. Factors affecting the accuracy of elemental analysis by transmission EELS. *Microsc. Microanal. Microstruct.* **2**, 203–213 (1991).

27. Torres, J., Zhu, Y., Liu, P., Lim, S. C. & Yun, M. Adhesion Energies of 2D Graphene and MoS2 to Silicon and Metal Substrates. *Phys. Status Solidi Appl. Mater. Sci.* **215**, 1–8 (2018).

28. Koenig, S. P., Boddeti, N. G., Dunn, M. L. & Bunch, J. S. Ultrastrong adhesion of graphene membranes. *Nat. Nanotechnol.* **6**, 543–546 (2011).

29. Palatinus, L. *et al.* Specifics of the data processing of precession electron diffraction tomography data and their implementation in the program PETS2.0. *Acta Crystallogr. Sect. B Struct. Sci. Cryst. Eng. Mater.* **75**, 512–522 (2019).

30. Egerton, R. F. Choice of operating voltage for a transmission electron microscope. *Ultramicroscopy* **145**, 85–93 (2014).

31. Henderson, R. Cryo-protection of protein crystals against radiation damage in electron and X-ray diffraction. *Proc. R. Soc. B Biol. Sci.* **241**, 6–8 (1990).

32. Glaeser, R. M. & Taylor, K. A. Radiation damage relative to transmission electron microscopy of biological specimens at low temperature: a review. *J. Microsc.* **112**, 127–138 (1978).

33. Li, X. *et al.* Electron counting and beam-induced motion correction enable near-atomic-resolution single-particle cryo-EM. *Nat. Methods* **10**, 584–590 (2013).

34. Meyer, J. C. *et al.* Accurate Measurement of Electron Beam Induced Displacement Cross Sections for Single-Layer Graphene. *Phys. Rev. Lett.* **108**, 196102 (2012).

35. Egerton, R. F. Mechanisms of radiation damage in beam-sensitive specimens, for TEM accelerating voltages between 10 and 300 kV. *Microsc. Res. Tech.* **75**, 1550–1556 (2012).

36. Jiang, N. Damage mechanisms in electron microscopy of insulating materials. *J. Phys. D. Appl. Phys.* **46**, 305502 (2013).

37. Cazaux, J. Correlations between ionization radiation damage and charging effects in transmission electron microscopy. *Ultramicroscopy* **60**, 411–425 (1995).

38. Egerton, R. F. Control of radiation damage in the TEM. *Ultramicroscopy* **127**, 100–108 (2013).

39. Hudry, D. *et al.* Interface Pattern Engineering in Core-Shell Upconverting Nanocrystals: Shedding Light on Critical Parameters and Consequences for the Photoluminescence Properties. *Small* **17**, 1–13 (2021).